Single virus detection from the reactive shift of a whispering-gallery mode

F. Vollmer[a,1], S. Arnold[b,1], and D. Keng[b]

[a]The Rowland Institute, Harvard University, Cambridge, MA 02142; and [b]MicroParticle PhotoPhysics Lab, Polytechnic Institute of New York University, Brooklyn, NY 11201

Edited by Robert H. Austin, Princeton University, Princeton, NJ, and approved November 10, 2008 (received for review September 9, 2008)

We report the label-free, real-time optical detection of Influenza A virus particles. Binding of single virions is observed from discrete changes in the resonance frequency/wavelength of a whispering-gallery mode excited in a microspherical cavity. We find that the magnitude of the discrete wavelength-shift signal can be sufficiently enhanced by reducing the microsphere size. A reactive sensing mechanism with inverse dependence on mode volume is confirmed in experiments with virus-sized polystyrene nanoparticles. By comparing the electromagnetic theory for this reactive effect with experiments, the size and mass ($\approx 5.2 \times 10^{-16}$ g) of a bound virion are determined directly from the optimal resonance shift.

biosensor | influenza | optical resonance

Virus particles are a major cause for human disease, and their early detection is of added urgency since modern day travel has enabled these disease agents to be spread through populations across the globe (1). Fast and early detection on site of an outbreak requires biosensors where ideally individual viral particles produce a quantitative signal. Here, we report the observation of discrete changes in frequency of whispering gallery modes (WGMs) as Influenza A virions bind to a microsphere cavity. A "reactive" perturbation of the resonant photon state is confirmed in measurements with similar-sized polystyrene (PS) particles near a wavelength of 1,310 nm: The frequency/wavelength shift signal follows a strong dependence on cavity curvature near the predicted $\sim R^{-5/2}$ scaling (2), providing a mechanism for increasing signal by limiting modal volume. By reducing the microsphere radius to just <40 μm and operating at a more favorable wavelength near 760 nm where reduced water absorption is expected to enhance sensitivity (3), binding steps of individual Influenza A (InfA) virions are seen that easily exceed the experimental noise level. Analytic equations are derived that relate discrete changes in resonance wavelength to the size and mass of adsorbed virions. Although field effect techniques using nanofibers (4) and interferometric approaches based on light scattering (5) have demonstrated single virion sensing in the past, reactive WGM sensing adds new dimensions to what can be learned: The measured wavelength shift enables one to quantitatively identify the virion size and mass.

Experimental Approach

WGM resonances are perturbed toward longer wavelength as particles with polarizability in excess to that of water adsorb to a microsphere cavity. Individual binding events have been theorized to produce discrete steps in a time-trace of the wavelength shift signal (2). To probe for single binding events we immerse a silica microsphere in a suspension of polystyrene particles (PS) with radius $a = 250$ nm (Fig. 1). The PS particles are diluted in PBS to final concentrations $\approx$10–50 fM. A tunable distributed feedback laser (DFB) ($\approx$1,311 nm nominal wavelength) excites WGMs by evanescent coupling from a tapered optical fiber. A WGM mode is detected as a Lorentzian-shaped trough in a spectrum acquired by a photodetector that measures transmission through the fiber as the wavelength of the laser is tuned (6). Fig. 1 *Inset* shows the typical transmission spectrum for a WGM excited in silica microsphere (here radius $R \approx 50$ μm) immersed in aqueous solution. The linewidth $\delta\lambda \approx 5$ pm, as determined from the full width at half-maximum, corresponds to a Q factor $Q = \lambda/\delta\lambda \approx 2.6 \times 10^5$, primarily limited by overtone vibrational absorption of water in the near infrared. Microspheres are fabricated from tapered optical fiber tips that are melted in a focused 10-W CO_2 laser (7). Immediately after fabrication, the microsphere-on-a-stem is mounted on the sample cell and immersed in PBS solution. A small box encloses the sample cell to limit air flow and stabilize the ambient humidity level. A transmission spectrum is acquired every $\approx$20 ms, and the resonance wavelength is determined from a parabolic minimum fit to the Lorentzian-line, typically with precision $\approx$1% of the linewidth. The dip-trace is displayed as fractional shift in wavelength $\Delta\lambda/\lambda$.

Fig. 2*A* shows a trace of $\Delta\lambda/\lambda$ for $a = 250$ nm PS particles interacting with a microsphere with $R \approx 45$ μm. Steps of various heights are clearly visible against the background cavity noise indicating adsorption of individual PS particles. We believe that the spikes such as those shown in Fig. 2*B* are associated with unsuccessful adsorption attempts. Fig. 2*C* shows the step statistics. A maximum step height can be distinguished. With the ability to detect discrete steps and identify optimal step height within a dip trace for a given nanoparticle radius, we can now direct our attention toward measuring the dependence of the optimal shift signal on the microsphere curvature. We experiment with different-sized microspheres ($R = 44$–105 μm) and plot maximum step heights versus curvature (i.e., $1/R$, Fig. 3). Interestingly, we find a strong dependence of the fractional wavelength shift on the cavity radius, scaling as $R^{-2.67}$. This is in good agreement with electromagnetic theory associated with reactive WGM sensing, for which steps have been predicted for single protein binding, with maximum step heights in proportion to $R^{-2.5}$ (2). The largest step heights are predicted for protein particles binding to the equator, whereas a $\sim 1/R$ dependence (2) is expected for a shift due to a random surface density. (6) The small discrepancy in the exponent (-2.67 vs. -2.5) in our PS particle experiments may be explained by an increase in the evanescent interaction caused by a slight lengthening in the evanescent field depth L as the microsphere size is decreased, and is associated with large particles adsorbed for which $a/L \approx 1$. For particles that are small compared with the evanescent field depth, such as protein or InfA virus, our optimal wavelength shifts are consistent with the reactive theory, but the weak signal

Author contributions: F.V. and S.A. designed research; F.V. performed research; F.V. contributed new reagents/analytic tools; F.V., S.A., and D.K. analyzed data; and F.V. and S.A. wrote the paper.

The authors declare no conflict of interest.

This article is a PNAS Direct Submission.

Freely available online through the PNAS open access option.

[1]To whom correspondence may be addressed. E-mail: vollmer@rowland.harvard.edu or arnold@photon.poly.edu.

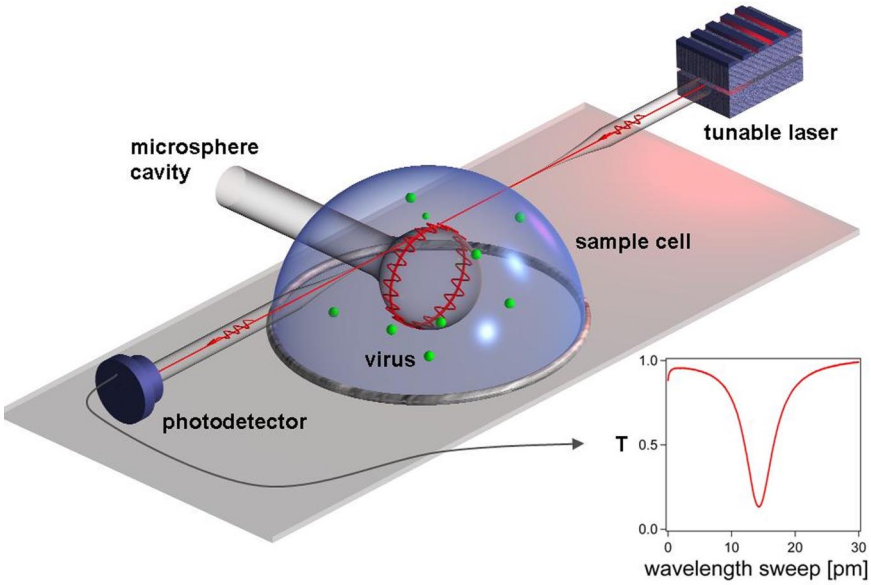

Fig. 1. Excitation of an equatorial WGM of a microsphere by evanescent coupling to a guided wave in a tapered optical fiber. Resonance positions are detected as dips in the transmitted light T at particular laser wavelengths.

associated with these smaller particles prohibits us from acquiring data over a wide range of microsphere sizes.

Having identified a means for increasing the shift magnitude by reducing microcavity size, we set out to optimize the microsphere system for the detection of single InfA virions. InfA virions have an average radius $a \approx 50$ nm (8) and a refractive index below that of PS. Although our microcavity fabrication method would allow us to take further advantage of the large curvature enhancement of the wavelength shift signal by forming smaller cavities, the success of this approach is limited: further reduction of cavity size also increases cavity leakage so that any gain in sensitivity due to shift enhancement is offset by a broadening of the resonance linewidth. Instead, we find that further increase in sensitivity is possible if we scale down the wavelength λ and the cavity. A wavelength $<$1,311 nm is also favorable due to less absorption in water. Following this approach, we use DFB laser with $\lambda \approx 763$ nm and excite a WGM with $Q \approx 6.4 \times 10^5$ in $R = 39$-μm microspheres. We inject InfA virions at concentration of $\approx$10 fM directly into a PBS filled sample cell, since the virions are known to adsorb to silica (9). The dip-trace of the resonance wavelength $\Delta\lambda_{InfA}/\lambda$ in Fig. 4 reveals clear steps associated with binding of single viral particles and one unbinding event. The signal-to-noise ratio ($\Delta\lambda_{InfA}/\Delta\lambda_{noise} \approx 3$) can be further improved upon by signal processing schemes such as Median filtering; the solid line in Fig. 4 shows a median filter of rank 3. A similar median filter has been applied in the green curve in Fig. 2*A*.

High-sensitivity measurements of individual virus particles are made possible by reducing modal volume, a principle that should also apply to other WGM cavity geometries (10) and other non-WGM microcavities (e.g., photonic crystals with "defects") (11). Below, we show that the steps heights already recorded for the microsphere geometry can be described analytically by using the reactive theory, and that the viral size and mass may be identified.

Reactive Sensing Mechanism

Reactive sensing relies on the fact that work is done by the evanescent field of a microcavity as a polarizable nanoparticle moves from a distant position to the microcavity surface. As a result, the energy of light in the resonator is reduced. With the number of cavity photons conserved, the frequency of each

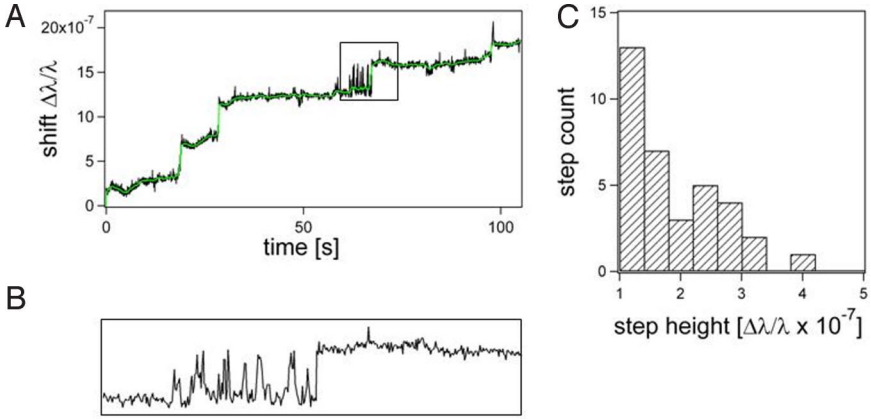

Fig. 2. Nanoparticle wavelength shift. (*A*) Dip-trace for $a = 250$ nm PS particles interacting with a microsphere with $R \approx 45$ mm. (*B*) A 15 second zoom-in. (*C*) Wavelength step statistics.

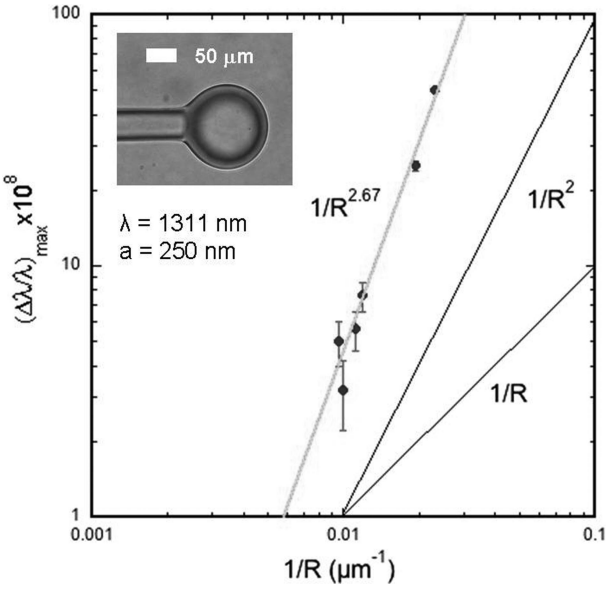

Fig. 3. Maximum step height vs. microsphere curvature for polystyrene particles with radius $a = 250$ nm.

resonant photon is shifted by $\Delta\omega_r$ in accordance with refs. 2 and 3.

$$\hbar\Delta\omega_r \cong -\frac{\alpha_{ex}}{2}\langle E(\boldsymbol{r}_v, t)^2\rangle, \qquad [1]$$

where $\langle E(\boldsymbol{r}_v, t)^2\rangle$ is the time average of the square of the field at the nanoparticle's position $\boldsymbol{r}_v$ due to a single photon resonant state. We have assumed that the particle is small in relation to the wavelength, and has an isotropic excess polarizability α_{ex} including local field effects. Under these conditions, Eq. **1** should work for any microcavity geometry. By dividing the shift in frequency by the single photon energy $\hbar\omega_r$ on the left and by the volume integral of the associated electromagnetic energy density on the right, we arrive at a simple expression for the fractional frequency shift (2),

$$\left(\frac{\Delta\omega_r}{\omega_r}\right) \cong \frac{-(\alpha_{ex}/\varepsilon_0)|\boldsymbol{E}_0(\boldsymbol{r}_v)|^2}{2\int \varepsilon_r(\boldsymbol{r})|\boldsymbol{E}_0(\boldsymbol{r})|^2 dV}, \qquad [2]$$

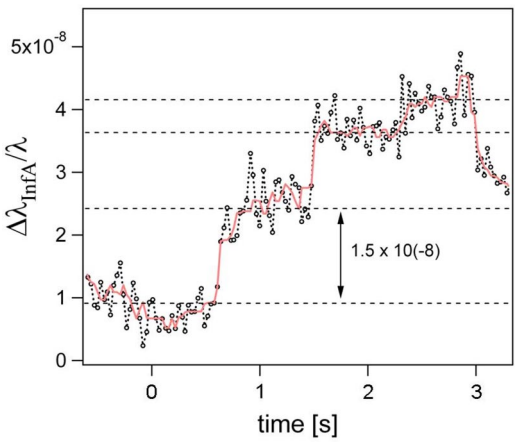

Fig. 4. Shift signal for InfA. The data were acquired for a microsphere with $R = 39$ mm, and a DFB laser having a nominal wavelength of 763 nm.

where $\boldsymbol{E}_0$ is the electric field amplitude, and $\varepsilon_r(\boldsymbol{r})$ is the dielectric constant throughout the cavity. Although the field in Eq. **1** is associated with a single photon, this restriction does not apply to Eq. **2**, since both the numerator and denominator are separately proportional to the number of photons; the reactive effect is independent of intensity. In addition, the volume integration in the denominator suggests that the reactive effect should vary inversely with volume. This insight although approximate, is none-the-less almost correct. In what follows we describe our theoretical results for the resonance shift of a microspherical cavity. From this point onward we will express the resonance shift as a shift in free space wavelength in accord with the experimental data (i.e., $\Delta\lambda_r/\lambda_r = -\Delta\omega_r/\omega_r$).

Evaluation of Eq. **2** for a microspherical cavity is most elegantly carried out for the lowest order WGM launched around the equator of a glass sphere of radius R.[2] Such a mode spreads symmetrically to either side of the equator with a Gaussian-like profile, causing nanoparticles adsorbing above or below the equator to have a diminished shift relative to the equatorial shift. The maximum shift (i.e., equatorial) for a nanoparticle of radius a_v adsorbing on the equator is found to be

$$\left(\frac{\Delta\lambda_r}{\lambda_r}\right)_{max} \cong D\frac{a_v^3}{R^{5/2}\lambda_r^{1/2}}e^{-a_v/L}, \qquad [3]$$

where L is the characteristic length of the evanescent field, and D is dimensionless dielectric factor* associated with both the microsphere and nanoparticle. The wavelength shift enhancement that results from the reduction in microsphere size is clearly seen in Eq. **3** to be proportional to $R^{-5/2}$, in good agreement with experiment (Fig. 3). The exponential factor on the right results from the variation of the evanescent field over the radius of the nanoparticle. One can invert this transcendental equation to obtain the radius a_v of the adsorbed particle;

$$a_v \cong \frac{a_0}{1-\frac{a_0}{3L}}, \qquad [4]$$

where a_0 is

$$a_0 \cong \frac{R^{5/6}\lambda_r^{1/6}}{D^{1/3}}\left(\frac{\Delta\lambda_r}{\lambda_r}\right)_{max}^{1/3}. \qquad [5]$$

Numerical studies indicate that Eq. **4** deviates from the exact solution to Eq. **3** by $<1\%$ for $a_v < 90$ nm, and $R > 30$ μm.

Discussion

Eq. **3** provides a clear statement with respect to the dependence of the wavelength shift on microsphere curvature, and our polystyrene experiments agree well with respect to the exponent. Further evidence for the reactive mechanism results by comparing the nominal radii of the particles used in our experiments with the radii arrived from the maximum measured wavelength shifts (using Eq. **4**). These results are summarized in the table. We note that our measurements agree well with Eq. **4** for $a <$ 250 nm. We also would like to point out that the estimate of radius is a lower limit since only few particles bind directly on the equator. The mass m_v of the InfA virion can now be evaluated from its volume times its density to be 5.2×10^{-16} g, in agreement with results for InfA's molecular weight found from the sedimentation in density gradients based on a statistical number of viruses ($\approx 3 \times 10^8$ g/mol) (12).

*$L \approx (\lambda/4\pi)(n_s^2 - n_m^2)^{-1/2}$ and $D = 2n_m^2(2n_s)^{1/2}(n_{np}^2 - n_m^2)/(n_s^2 - n_m^2)(n_{np}^2 + 2n_m^2)$, where n_s, n_m, and n_{np} are the refractive indices of the microsphere (1.45), aqueous medium (1.33), and nano-particle (1.5 for virus and 1.59 for polystyrene).

Table 1. Measurement of size and mass for different particles

Particle, radius	Wavelength (λ), nm	Cavity radius (R), μm	Max. expt. step, $(\Delta\lambda/\lambda)_{max}$	Radius from Eq. **4** (a), nm
PS, 250 nm, $\sigma < 5\%$	1,311	44	5×10^{-7}	211
PS, 100 nm, $\sigma < 5\%$	763	30	2.2×10^{-7}	100
InfA, SEM* 45–55 nm	763	39	1.5×10^{-8}	47

SEM, scanning electron microscope.

Conclusions

We have shown that adsorption of individual nanoparticles produce discrete changes in resonance frequency/wavelength of a WGM. We confirm the reactive sensing mechanism (Eq. **1** and **2**) and use its signal enhancement by reducing the size of microspherical cavities. Detection of individual InfA virions in aqueous buffer is then demonstrated directly from steps in the wavelength shift signal. Both the virus size and mass are identified from maximum step height associated with binding near the equator. This work may be considered a forerunner for reactive biosensing with microcavities of ultrasmall modal volume such as "defects" within photonic crystals (11), since the Eq. **1** and **2** should still apply.

The number of attempts needed to bind is a direct reflection of the affinity of the bioparticle to a surface. No effort has been made in this first demonstration to extract ligand-receptor affinities, however, such experiments will be soon to follow. In addition the tumbling of a nearly spherical virus is not expected to lead to significant time dependent variations in the wavelength shift signal, however, rod like virus will couple through a tensor (3) interaction to the electromagnetic field and should lead to significant time variations, allowing one to gain more details concerning affinities associated with orientation. Fortunately, our approach has considerable bandwidth since a WGM can sense temporal variations down to the photon life $\tau = Q/\omega$, which is $\approx 10^{-10}$ s for the Q values reported in the current work. Furthermore, the genus of a virus may be determined from measurements that are sensitive to a virion's shape in addition to its size and mass. Considering the quantitative nature of the physical interaction, and its large available bandwidth, the future of single particle reactive WGM experiments is expected to be expansive. The approach based on microspheres has advantages over other cavity geometries and label-free sensing mechanisms where a closed-form analysis of the wavelength shift signal may not be possible (13).

Methods

Purified and formalin-inactivated human InfA virus A/PR/8/34 is purchased in 4-(2-hydroxyethyl)-1-piperazineethanesulfonic acid (Hepes) buffer from Charles River Laboratories. The virus sample is passed through a 0.2 μm nylon filter to remove aggregates and then concentrated in a speed vac. WGM sample cells (Fig. 1) are assembled from *o*-rings (McMaster–Carr, 12.5 mm diameter) glued to a 48 $\times$ 65 mm no. 1 coverslip (Gold Seal). A microsphere-on-a-stem is then glued to the *o*-ring so that the sphere resides in the center of the cell without touching the coverslip. The sample cell is mounted on an inverted microscope and visually inspected. The midsection of a tapered optical fiber, which is held between the posts of a u-shaped metal holder, is positioned in contact with the equator of the sphere (Fig. 1), using micrometer screws. Alignment is adjusted by optimizing the coupling to WGM modes by slightly moving the point-of-contact between taper and sphere within the equatorial region. To check for viral aggregates and estimate concentration, an aliquot of the purified virion solution is stained with DiIC membrane dye (Invitrogen) and fluorescently imaged using a cooled charge-coupled device (CCD) camera (Cooke). Similarly, fluorescent carboxylated polystyrene particles (Invitrogen) are checked for aggregates before use. Microspheres of controllable size are fabricated from tapered optical fiber (Corning; SMF-28). The taper is held on a stage above a reflecting Aluminum surface and melted in the focal spot of a focused 10-W CO_2 laser (Synrad). The process is inspected on a CCD camera while progressively more silica can be melted by pushing more fiber into the beam where surface tension immediately forms a sphere. Tapered SMF-28 fiber for evanescent coupling to microspheres is fabricated by pulling of the fiber on a motorized stage while softening its midsection in a butane/nitrous-oxide flame (Microtorch; Azure Moon Trading Corp.). The taper is typically $\approx$5 cm in length with a thinnest diameter $\approx$2 μm for coupling at $\approx$ 760 nm wavelength. DFB lasers are purchased from Thorlabs (1,311 nm wavelength) and Eagleyard (763 nm wavelength) and optically isolated (isolators purchased from Thorlabs and OFR). A free-space coupler (Thorlabs) equipped with a 20x objective is used to couple to the SMF-28 fiber. ILX Lightwave controllers are used to tune the laser diode by sweeping the current with a sawtooth-shaped function.

ACKNOWLEDGMENTS. This work was supported by a Rowland Junior Fellowship (to F.V.) and National Science Foundation Division of Bioengineering and Environmental Systems Grant 0522668 (S.A.).

1. P.W. Ewald (2002) In *The Next Fifty Years*, ed Brockman J (Vintage Books, New York), pp 289–301.
2. Arnold S, Khoshsima M, Teraoka I, Holler S, Vollmer F (2003) Shift of whispering gallery modes in microspheres by protein adsorption. *Opt Lett* 28:272–274.
3. Arnold S, Ramjit R, Keng D, Kolchenko V, Teraoka I (2008) Microparticle photophysics illuminates viral biosensing. *Faraday Discuss* 137:65–85.
4. Patolsky F, *et al.* (2004) Electrical detection of single viruses. *PROC NATL ACAD SCI USA* 101:14017–14022.
5. Ignatovich FV, Novotny L (2006) Real-time and background-free detection of nanoscale particles. *Phys Rev Lett* 96:0139011–0139014.
6. Vollmer F, *et al.* (2002) Protein detection by optical shift of a resonant microcavity. *Appl Phys Lett* 80:4057–4059.
7. Collot L, Lefevre-Seguin V, Brune M, Raimond JM, Haroche S (1993) Very high-Q whispering-gallery mode resonances observed on fused silica microspheres. *Europhys Lett* 25:327–334.
8. Lamb RA, Krug RM (2001) In *Fundamental Virology*, eds Knipe DM, Howley PM (Lippincott Williams & Wilkins, Philadelphia), pp 725–728.
9. Bresler SE, *et al.* (1975) Purification of influenza-viruses on wide-pore glass columns. *Acta Virologica* 19:190–196.
10. Vollmer F, Arnold S (2008) Whispering-gallery mode Biosensing: Label-free detection down to single molecules. *Nat Methods* 5:591–596.
11. Song BS, Noda S, Asano T, Akahane Y (2005) Ultra-high-Q photonic double-heterostructure nanocavity. *Nat Mater* 4:207–210.
12. Reimer CB, Baker RS, Newlin TE, Havens ML (1966) Influenza virus purification with the zonal ultracentrifuge. *Science* 3:1379–1381.
13. Armani AM, Kulkarni RP, Fraser SE, Flagan RC, Vahala KJ (2007) Label-free, single-molecule detection with optical microcavities. *Science* 317:783–787.